J. Cell. Mol. Med. Vol 21, No 10, 2017 pp. 2514-2523

# Class III antiarrhythmic drugs amiodarone and dronedarone impair $K_{IR}2.1$ backward trafficking

**Yuan Ji [a], Hiroki Takanari [a], Muge Qile [a], Lukas Nalos [b], Marien J.C. Houtman [a], Fee L. Romunde [a], Raimond Heukers [c], Paul M.P. van Bergen en Henegouwen [c], Marc A. Vos [a], Marcel A.G. van der Heyden [a,] ***

[a] *Division of Heart & Lungs, Department of Medical Physiology, UMCU, Utrecht, The Netherlands*
[b] *Department of Physiology, Faculty of Medicine in Pilsen, Charles University in Prague, Pilsen, Czech Republic*
[c] *Cell Biology, Department of Biology, Science Faculty, Utrecht University, Utrecht, The Netherlands*

*Received: November 23, 2016; Accepted: February 24, 2017*

## Abstract

Drug-induced ion channel trafficking disturbance can cause cardiac arrhythmias. The subcellular level at which drugs interfere in trafficking pathways is largely unknown. $K_{IR}2.1$ inward rectifier channels, largely responsible for the cardiac inward rectifier current ($I_{K1}$), are degraded in lysosomes. Amiodarone and dronedarone are class III antiarrhythmics. Chronic use of amiodarone, and to a lesser extent dronedarone, causes serious adverse effects to several organs and tissue types, including the heart. Both drugs have been described to interfere in the late-endosome/lysosome system. Here we defined the potential interference in $K_{IR}2.1$ backward trafficking by amiodarone and dronedarone. Both drugs inhibited $I_{K1}$ in isolated rabbit ventricular cardiomyocytes at supraclinical doses only. In HK-KWGF cells, both drugs dose- and time-dependently increased $K_{IR}2.1$ expression (2.0 $\pm$ 0.2-fold with amiodarone: 10 $\mu$M, 24 hrs; 2.3 $\pm$ 0.3-fold with dronedarone: 5 $\mu$M, 24 hrs) and late-endosomal/lysosomal $K_{IR}2.1$ accumulation. Increased $K_{IR}2.1$ expression level was also observed in the presence of $Na_v1.5$ co-expression. Augmented $K_{IR}2.1$ protein levels and intracellular accumulation were also observed in COS-7, END-2, MES-1 and EPI-7 cells. Both drugs had no effect on $K_v11.1$ ion channel protein expression levels. Finally, amiodarone (73.3 $\pm$ 10.3% $P < 0.05$ at $-120$ mV, 5 $\mu$M) enhanced $I_{KIR2.1}$ upon 24-hrs treatment, whereas dronedarone tended to increase $I_{KIR2.1}$ and it did not reach significance (43.8 $\pm$ 5.5%, $P = 0.26$ at $-120$ mV; 2 $\mu$M). We conclude that chronic amiodarone, and potentially also dronedarone, treatment can result in enhanced $I_{K1}$ by inhibiting $K_{IR}2.1$ degradation.

**Keywords:** inward rectifier • $K_{IR2.1}$ • degradation • lysosome • amiodarone • dronedarone

## Introduction

Proper ion channel expression and function is one of the cornerstones of normal heart function. Unequal ion distribution between the intra-and extracellular compartment in concert with ion specific voltage-sensitive channels in the plasma membrane determines action potential formation. The stable and negative resting membrane potential in between action potentials results from the activity of the inward rectifying ion channels of the *KCNJ* gene family [1]. In the heart, the $K_{IR}2.1$ channel protein, encoded by *KCNJ2*, is the main contributor to ventricular $I_{K1}$. $K_{IR}2.1$ loss of function has been associated with Andersen–Tawil syndrome, characterized by action potential prolongation, and thus QT-lengthening on the ECG. Furthermore, patients experience periodic paralysis and mild episodes of cardiac arrhythmia [2]. In contrast, gain-of-function mutations are associated with QT shortening and atrial fibrillation [3]. Besides its important function in the heart, $K_{IR}2.1$ proteins also contribute to inward rectifier currents in skeletal and smooth muscle, and several neuronal cell types [4]. In Andersen–Tawil syndrome patients, association with the occurrence of increased U-waves on the ECG has been found [5]. Pharmacological inhibition of KCNJ channels by barium has also been associated with more apparent U-waves [6]. In a study on the presence and amplitudes of U-waves associated with loss- and gain-of-function mutations in KCNJ2 patients at normokalemic conditions, the authors speculate that at least a part of the U-wave is inversely correlated with the amount of $I_{K1}$ [7].

$K_{IR}2.1$ ion channel trafficking is a strictly regulated process that can be divided into forward (anterograde; towards the plasma membrane) and backward (retrograde; from the plasma membrane) trafficking events [8]. $K_{IR}2.1$ channels become internalized *via* a clathrin-mediated pathway and subsequently travel towards the lysosome, where the channels ultimately become degraded *via* an initial discrete

*Correspondence to: Marcel A.G. VAN DER HEYDEN, Ph.D.
E-mail: m.a.g.vanderheyden@umcutrecht.nl

doi: 10.1111/jcmm.13172

cleavage step that removes the N-terminus [9, 10]. Interference in lysosomal degradation and upstream trafficking events by specific inhibitors results in increased $K_{IR}2.1$ expression levels, and most likely by saturation of the endocytotic machinery, also in increased $I_{K1}$ densities [9, 10]. Also clinical drugs can have significant effects on ion channel trafficking and this can lead to severe adverse effects [8]. Among the variety of affected channel proteins, the $K_{IR}2.1$ channel internalization and degradation is sensitive for disturbances by, although old, clinical drugs like chlorpromazine and chloroquine [9–11].

Amiodarone is a class III antiarrhythmic, based on the benzofuran structure used in atrial and ventricular fibrillation therapy [12]. Amiodarone is a multichannel blocker affecting delayed rectifier $I_{Kr}$, sodium channel and L-type calcium currents. Amiodarone therapy is known for its many adverse effects on the ocular, neurological, dermatological, thyroid, gastrointestinal, pulmonary, cardiac and liver systems [13–15]. Some studies demonstrate detrimental effects of amiodarone on cargo trafficking through the late-endosome/lysosome compartments, which could partly explain the plethora of side effects [16–18]. Amiodarone has been shown to inhibit the degradation of lung surfactant protein A *in vitro* and *in vivo* [16]. Dronedarone is a synthetic analogue of amiodarone developed to preserve antiarrhythmic properties with less adverse effects, especially thyroid and pulmonary toxicity [19]. Compared with amiodarone, dronedarone is less lipophilic and has a much shorter half-life (1–2 *versus* 30–55 days). Nevertheless, also dronedarone appears to interfere in normal late-endosome/lysosome function [17]. Chronic amiodarone therapy has been associated with the appearance of prominent U-waves [20–22], which may allude to a potential disturbance of $I_{K1}$. Currently, it is unknown whether amiodarone and dronedarone interfere in the process of $K_{IR}2.1$ trafficking, in particular its degradation, which was therefore investigated in the current study.

# Materials and methods

## Rabbit ventricular cardiomyocyte isolation

Animal care and experimental procedures were in accordance with the 'European Directive for the Protection of Vertebrate animals used for Experimental and Scientific Purpose, European Community Directive 2010/63/EU' and were approved by the Committee for Experiments on Animals of the Utrecht University, the Netherlands.

Ventricular rabbit cardiomyocytes were isolated by enzymatic digestion using a Langendorff set-up identical to that described previously [23].

## Cell culture

HEK293 cells expressing C-terminal GFP-tagged murine $K_{IR}2.1$ (HK-KWGF cells) were cultured as described before [9, 24]. Mouse P19 embryonal carcinoma-derived germ layer cell lines END-2, MES-1 and EPI-7 cells [25, 26], COS-7, HEK293t, HEK-hERG [27] and Ex-293 [28] cells were cultured in DMEM (Lonza, Breda, the Netherlands) supplemented with 10% FCS (Sigma-Aldrich, Zwijndrecht, the Netherlands), 2 mM L-glutamine (Lonza), and 50 U/ml penicillin and 50 mg/ml streptomycin (both Lonza). In time course experiments, cells were seeded and harvested on identical days.

In COS-7 western blot experiments, cells were transfected using linear polyethylenimine (PEI). In short, PEI (Mw 25,000 Polysciences Inc., Eppelheim, Germany) was dissolved in water at 0.323 g/l. PEI solution was subsequently adjusted to pH 8.0, sterilized using filtration and freeze-thawed four times. Aliquots of PEI stock solution were stored at −20°C. For each transfection, 2.5 μg plasmid DNA was added to a 150 mM NaCl solution, total volume 150 μl. 20 μl of PEI stock solution was also added to a 150 mM NaCl solution, total volume 150 μl. Both solutions were mixed, incubated at room temperature for 20 min. and subsequently added to the cells. Medium was replaced at 16 hrs post-transfection. In immunofluorescence microscopy experiments, HEK293t, END-2, MES-1 and EPI-7 cells were transfected with human $K_{IR}2.1$ + Rab7-GFP or $K_{IR}2.1$ alone using Lipofectamine (Invitrogen, Breda, the Netherlands) according to the manufacturer's protocol.

## Drugs

Amiodarone (cat. no. 8357 lot AR20569) and dronedarone (cat. no. SR33589B lot 7963) (both Sanofi Recherche, Montpellier, France) were dissolved in DMSO at 50 mM.

## Immunohistochemistry and confocal microscopy

HK-KWGF cells were cultured on Ø 15-mm cover slips, pre-coated with poly-L-lysine (Sigma-Aldrich). END-2, MES-1, EPI-7 and HEK293t cells were cultured on Ø 15-mm cover slips, pre-coated with 0.1% gelatin. Cells were rinsed with PBS supplemented with 1 mM $Ca^{2+}$ and 1 mM $Mg^{2+}$ and fixed with 3% paraformaldehyde, pH 7.4. Permeabilization was performed with 0.5% Triton X-100 in PBS and 50 mM PBS–glycine was used as quenching agent. To block non-specific interaction sites, NET-gel was applied on the cells. Then cells were incubated overnight with the primary antibodies $K_{IR}2.1$ (for END-2, MES-1, EPI-7 and HEK293t cells (1:250; Santa Cruz Biotechnology, Heidelberg, Germany, cat. no. sc-18708), LAMP-1 (1:200; BD Bioscience Pharmingen, Breda, The Netherlands) or EEA1 (1:1000; BD Bioscience Pharmingen) (both for HK-KWGF cells) in NET-gel. Cell nuclei were stained with 40,6-diamidino-2-phenylindole (DAPI) (1:50.000; Molecular Probes, Leiden, The Netherlands) during secondary antibody incubation. A five times 5 min. wash step procedure was done with NET-gel before and after incubation with donkey antimouse DyLight secondary antibody (1:250; Jackson ImmunoResearch Laboratories Inc., West Baltimore Pike West Grove, PA, USA) or donkey anti-goat Alexa Red (1:400; Jackson ImmunoResearch Laboratories Inc.). The cover slips were mounted with Vectashield (Vector Laboratories Inc. Burlingame, CA, USA), and confocal images were obtained using a Zeiss Axiovert 200 M confocal microscope (Carl Zeiss Microscopy GmbH, Germany) equipped with a 63× water immersion objective (NA 1.2) plus 2× digital zoom. Excitation was performed with an air-cooled Argon ion laser (LASOS, RMC 7812Z, 488 nm) for GFP and a HeNE (LASOS, SAN 7450A, 543 nm) laser for DyLight. Colocalization between $K_{IR}2.1$-GFP, EEA1, and LAMP-1, and $K_{IR}2.1$ and Rab7-GFP, was quantified by determining the Pearson coefficient ($r$) with the Costes automated threshold method provided by the JACoB plugin for the ImageJ software [29].



Journal of Cellular and Molecular Medicine published by John Wiley & Sons Ltd and Foundation for Cellular and Molecular Medicine.

## Western blotting

Following treatment, cells were harvested in lysis buffer (20 mM HEPES, pH 7.6, 125 mM NaCl, 10% (v/v) glycerol, 1 mM EDTA, 1 mM EGTA, 1 mM dithiothreitol, 1% (v/v) Triton X-100). Subsequently, 20 μg protein lysate was separated by 7% or 10% SDS-PAGE and blotted onto nitrocellulose membrane. Blots were blocked with 5% (w/v) non-fat milk powder for detection with GFP antibody (1:500; Santa Cruz Biotechnology, cat. no. sc9996) or $K_v$11.1 antibody (1:3000; Alomone Labs, Jerusalem, Israel, cat. no. APC062) or 5% egg yolk (v/v) for $K_{IR}$2.1 antibody (1:250; Santa Cruz Biotechnology, cat. no. sc-18708) in TBST (20 mM Tris–Cl, pH 8.0, 150 mM NaCl, 0.05% (v/v) Tween-20) for 1 hr at room temperature. Donkey antimouse or anti-goat (Jackson ImmunoResearch, cat. nos. 715-065-137 and 705-035-003, respectively) horseradish peroxidase secondary antibody was subsequently used. Standard ECL Prime procedure was used for final detection (GE Healthcare Life Sciences, Eindhoven, the Netherlands).

## Electrophysiology

In ventricular rabbit cells, $I_{K1}$ was measured by patch clamp experiments in whole-cell mode using an Axon amplifier controlled by pClamp9.2 software (Molecular Devices, Sunnyvale, CA, USA). Experiments were performed at 37°C using temperature control (Cell MicroControls, Norfolk, VA, USA). Cardiomyocytes were put in the chamber and superfused with normal Tyrode's solution (mM) (140 NaCl, 5 KCl, 6 HEPES, 6 glucose, 1.8 $CaCl_2$, 1 $MgCl_2$, pH 7.4 with NaOH). Borosilicate glass pipettes were made with a Sutter P-2000 puller (Sutter Instrument, Novato, CA, USA) and had a pipette resistant of 2–3 MΩ when filled with pipette solution (mM) (110 KCl, 10 EGTA, 10 HEPES, 4 $K_2$-ATP, 5.17 $CaCl_2$, 1.42 $MgCl_2$, pH 7.2 with KOH). The voltage protocol for $I_{K1}$ measurements was as follows: holding potential was set to −80 mV, and a prepulse at −40 mV for 200 ms was applied to inactivate native sodium current. $I_{K1}$ was elicited by 1-s step pulses from −120 mV to 30 mV by 10 mV step increments.

HK-KWGF cells were grown on 0.1% gelatin (Bio-Rad, Veenendaal, the Netherlands) coated Ø 12-mm cover slips. $I_{KIR2.1}$ from single cells was recorded in whole-cell voltage clamp mode using an Axopatch 200B amplifier and a Digidata 1322A digitizer and recorded with pCLAMP 9.2 software. Signals were low-pass-filtered at 2 kHz and sampled at 4 kHz. Measurements were taken at 37°C in a temperature-controlled perfusion chamber filled with tyrode solution containing (in mM) NaCl 140, KCl 5.4, $CaCl_2$ 1.8, $MgCl_2$ 1, glucose 6, HEPES 6, pH 7.4/NaOH. Pipettes were pulled on a Sutter Instrument P-2000 laser micropipette puller and had a resistance of 1.5–3 MΩ when filled with pipette solution, containing (in mM) K-gluconate 125, KCl 10, EGTA 5, $CaCl_2$ 0.6, $MgCl_2$ 2, HEPES 5, $Na_2ATP$ 4, pH 7.2/KOH. HK-KWGF cells were kept at a holding potential of -40 mV and 1-s test pulses were applied ranging from −120 mV to +30 mV with increments of 10 mV.

Steady-state currents from both cell types were analysed using Clampfit 9.2 software (Molecular Devices) and corrected for membrane capacitance to determine current density.

## Statistics

Data were analysed using GraphPad Prism version 6.00 for Windows (GraphPad Software, La Jolla, California USA) or Origin 8 (Microcal Software, Northampton, MA, USA) for rabbit cardiomyocyte measurements. For normally distributed data, Student's *t*-test or ANOVA for paired samples with Tukey's HSD post hoc or Bonferroni correction for multiple comparisons was used, while nonparametric data were analysed using Wilcoxon rank-sum test and Friedman's test with Dunn's multiple comparison test. Results are presented as mean ± S.E.M. Values of $P < 0.05$ were considered significant.

# Results

Amiodarone and dronedarone are known to have $I_{K1}$ blocking capacities in guinea pig ventricular cardiomyocytes [30, 31], albeit that their respective $IC_{50}$ values of >20 μM and >30 μM are beyond maximal plasma levels obtained from patients (approximately 5 μM for amiodarone and 0.3 μM for dronedarone) [19, 32]. Using rabbit ventricular cardiomyocytes, we were able to confirm these results as depicted in Figure 1A and B. Block at −120 mV was 17.0 ± 1.4%, 25.4 ± 4.0% and 54.3 ± 7.2% for 5, 10 and 50 μM amiodarone, respectively. Outward current block at −80 mV was 17.5 ± 2.3% and 35.7 ± 6.0% for 10 and 50 μM amiodarone, respectively. Similar levels of inhibition were observed with dronedarone (block at −120 mV of 17.6 ± 2.5%, 28.4 ± 3.6% and 46.2 ± 6.3%; block at −80 mV of 2.3 ± 0.3%, 15.1 ± 2.8% and 40.1 ± 7.0% for 1, 5 and 20 μM, respectively).

We next assessed effects of chronic treatment with amiodarone and dronedarone on $K_{IR}$2.1 expression in our previously described model system for $K_{IR}$2.1 channel trafficking, HK-KWGF cells [9–11]. Both amiodarone and dronedarone resulted in dose-dependent increase in total $K_{IR}$2.1 expression as established by Western blotting (Fig. 2A and B). In these assays, the strongest effects were reached with 20 μM amiodarone (2.9 ± 0.2-fold) and 10 μM dronedarone (6.1 ± 1.5), respectively. No effects on mRNA levels were found by quantitative PCR (1.00 ± 0.02 *versus* 0.92 ± 0.02 and 1.02 ± 0.01 for control, 10 μM amiodarone and 5 μM dronedarone, respectively). In contrast, amiodarone and dronedarone were unable to increase mature and immature $K_v$11.1 expression in stably transfected HEK293 cells (Fig. 2C and D).

Finally, we tested whether increased $K_{IR}$2.1 expression levels are dependent upon coexpression of $Na_v$1.5 expression, a cardiac ion channel that has previously been shown to associate with $K_{IR}$2.1 and which combined expression demonstrates reciprocal modulation [33]. Ex-293 cells, a HEK293 cell line both expressing $K_{IR}$2.1 and $Na_v$1.5 [28], displayed a dose-dependent increase in $K_{IR}$2.1 expression upon treatment with either amiodarone or dronedarone (Fig. 2E and F). Strongest effects were observed with 20 μM amiodarone (3.4 ± 1.2-fold) and 10 μM dronedarone (14.44 ± 6.0).

To determine whether the increased $K_{IR}$2.1-GFP expression levels is cell line specific or depends on the GFP tag, experiments were repeated in transiently transfected COS-7 cells. Under these conditions, similar effects were seen for amiodarone and dronedarone on the non-tagged human $K_{IR}$2.1 (Fig. 3A and B). Strongest effects in COS-7 cells were observed with 20 μM amiodarone (3.4 ± 0.6-fold) and 10 μM dronedarone (4.5 ± 0.7).

Significant enhanced expression of $K_{IR}$2.1 in HK-KWGF cells was seen from 4 hrs following drug application. Maximal response rates were observed after 4–6 hrs (Fig. 4A and B).

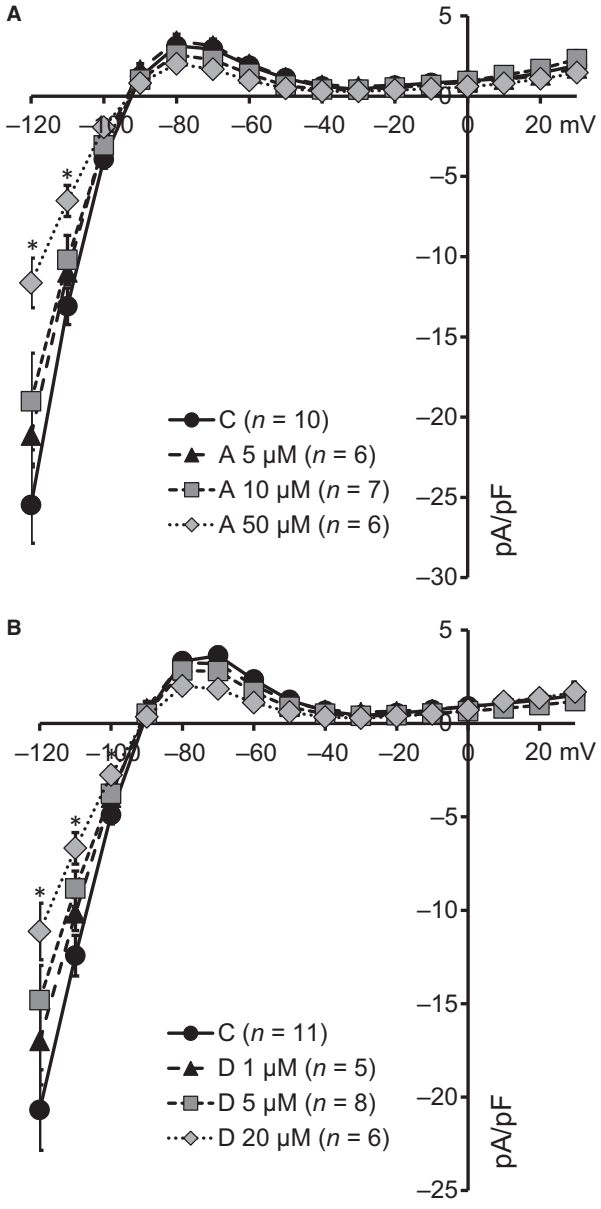


**Fig. 1** Acute application of supraclinical concentrations of amiodarone and dronedarone inhibits $I_{k1}$ in rabbit left ventricular cardiomyocytes. (**A**) $I_{K1}$ current–voltage relationships of cardiomyocytes superfused with 5 μM (triangles, $N = 6$), 10 μM (squares, $N = 7$) and 50 μM (diamonds, $N = 6$) amiodarone (A) display dose-dependent decreases in $I_{K1}$ reaching significance for 50 μM (at −120 and −110 mV) only. C depicts time-matched controls ($N = 10$). (**B**) $I_{K1}$ current–voltage relationships of cardiomyocytes superfused with 1 μM (triangles, $N = 5$), 5 μM (squares, $N = 8$) and 20 μM (diamonds, $N = 6$) dronedarone (D) display dose-dependent decreases in $I_{K1}$ reaching significance for 20 μM (at −120, −110 and −100 mV) only. C depicts time-matched controls ($N = 11$). *$P < 0.05$.

Immunofluorescence microscopy revealed dose-dependent accumulation of $K_{IR}2.1$-GFP (Fig. 5A) in a pattern resembling that of bafilomycin A1 and chloroquine treatment [10]. No intracellular accumulation was seen with 2 μM amiodarone or dronedarone, while relatively small aggregates were seen with 5 μM amiodarone and large aggregates were observed with 10 μM amiodarone or 5 μM dronedarone (Fig. 5A). In order to exclude that $K_{IR}2.1$-GFP accumulation in response to amiodarone and dronedarone is cell type specific or depends on the GFP tag, we made use of mouse P19 embryonal carcinoma-derived END-2, MES-1 and EPI-7 cells representing the three different germ layers [34] that were transiently transfected with non-tagged human $K_{IR}2.1$. Amiodarone at 10 μM induced clear intracellular aggregates similar as observed in HK-KWGF cells (Fig. 5B). Furthermore, dronedarone at 5 μM induced intracellular $K_{IR}2.1$ accumulation in MES-1 cells. In END-2 and EPI-7 cells, dronedarone appeared to induce larger aggregates (Fig. 5B).

An increase in $K_{IR}2.1$-GFP costaining for lysosomes (LAMP1) was observed following 10 μM amiodarone or 5 μM dronedarone (Pearson coefficient $0.13 \pm 0.02$, $0.56 \pm 0.03$ ($P < 0.05$) and $0.58 \pm 0.01$ ($P < 0.05$) for control, 10 μM amiodarone and 5 μM dronedarone, respectively) (Fig. 6A). Costaining for early endosomes (EEA1) revealed no increase in colocalization following 10 μM amiodarone ($0.10 \pm 0.06$ *versus* $0.18 \pm 0.07$ (n.s.) for control and 10 μM amiodarone) (Fig. 6B). In cells cotransfected with non-tagged $K_{IR}2.1$ and Rab7-GFP (late endosome), no change in colocalization was observed in response to 10 μM amiodarone or 5 μM dronedarone (Pearson coefficient $0.49 \pm 0.08$, $0.54 \pm 0.06$ (n.s.) and $0.51 \pm 0.07$ (n.s.) for control, 10 μM amiodarone and 5 μM dronedarone, respectively) (Fig. 6C).

We suggested that the intracellular accumulation of $K_{IR}2.1$-GFP protein could result in saturation of upstream trafficking pathways which may result in enhanced current levels, as seen before with the lysosomal inhibitor chloroquine [9] and the clathrin-mediated internalization inhibitor dynasore [10]. Cells were treated for 24 hrs with either 2 μM dronedarone or 5 μM amiodarone, and $I_{K1}$ densities were compared to their non-treated counterparts (Fig. 7A and B). Chronic dronedarone treatment resulted in a slight trend towards increased $I_{KIR2.1}$ densities for the inward ($43.8 \pm 5.5\%$, $P = 0.26$ at −120 mV) and a non-significant increase in outward ($32.0 \pm 7.8\%$, $P = 0.83$ at −60 mV) current components. 24-hrs treatment with amiodarone resulted in a significant increase in the inward current component at −120, −110 and −100 mV of $73.3 \pm 10.3\%$, $78.0 \pm 10.9\%$ and $84.4 \pm 11.5\%$, respectively, whereas a non-significant increased outward current ($75.9 \pm 24.9\%$, $P = 0.38$ at −60 mV) was observed.

## Discussion

Amiodarone is known for its hepatic and pulmonary adverse effects in patients. This is associated with the occurrence of lysosomal structural abnormalities such as lamellar lysosomal inclusion bodies [35, 36]. Less is known on the effects of amiodarone on muscle cell lysosome morphology and function. Several case reports demonstrate



Journal of Cellular and Molecular Medicine published by John Wiley & Sons Ltd and Foundation for Cellular and Molecular Medicine.

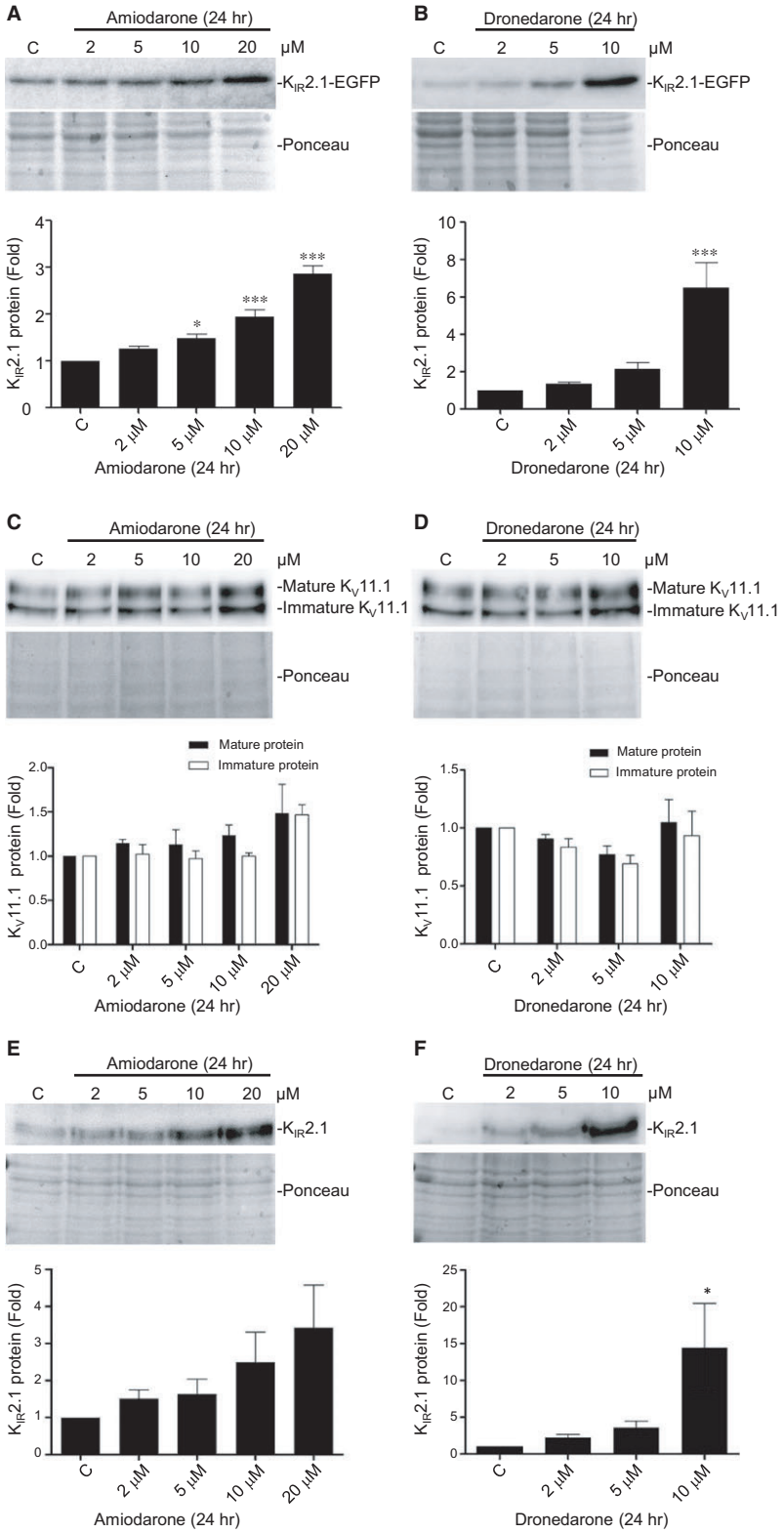


**Fig. 2** Amiodarone and dronedarone induce dose-dependent increases in $K_{IR}2.1$-GFP expression, independent of $Na_V1.5$ expression whereas $K_V11.1$ expression levels are not affected. (**A** and **B**) Western blot analysis of $K_{IR}2.1$-GFP expression in HK-KWGF cells treated with 2, 5, 10 or 20 μM amiodarone or 2, 5 or 10 μM dronedarone for 24 hrs. C indicates control (untreated) cells. Ponceau staining is used as loading control. Averaged data from eight (amiodarone) and seven (dronedarone) independent experiments, respectively, are depicted in bar graphs in the lower part of both panels.(**C** and **D**) Western blot analysis of $K_V11.1$ expression in HEK-hERG cells treated with 2, 5, 10 or 20 μM amiodarone or 2, 5 or 10 μM dronedarone for 24 hrs. C indicates control (untreated) cells. Ponceau staining is used as loading control. Averaged data from 3 independent experiments are depicted in bar graphs in the lower part of both panels. (**E** and **F**) Western blot analysis of $K_{IR}2.1$ expression in Ex293 cells treated with 2, 5, 10 or 20 μM amiodarone or 2, 5 or 10 μM dronedarone for 24 hrs. C indicates control (untreated) cells. Ponceau staining is used as loading control. Averaged data from three (amiodarone) and five (dronedarone) independent experiments are depicted in bar graphs in the lower part of both panels. $*P < 0.05$; $***P < 0.001$.

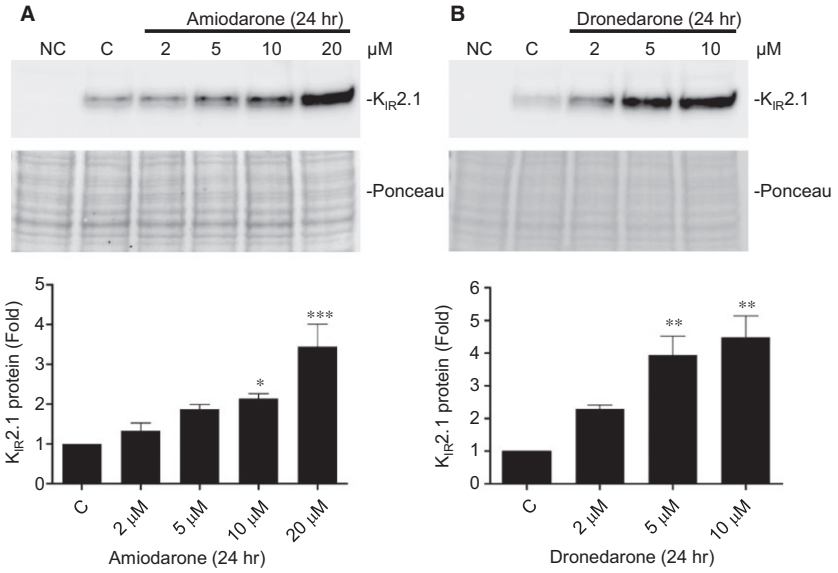


**Fig. 3** Amiodarone and dronedarone induce dose-dependent increases in $K_{IR}2.1$ expression in COS-7 cells. (**A** and **B**) Western blot analysis of $K_{IR}2.1$ expression in COS-7 cells treated with 2, 5, 10 or 20 μM amiodarone or 2, 5 or 10 μM dronedarone for 24 hrs. C indicates control (untreated) cells. Ponceau staining is used as loading control. Averaged data from three independent experiments are depicted in bar graphs in the lower part of both panels. $*P < 0.05$; $**P < 0.01$; $***P < 0.001$.

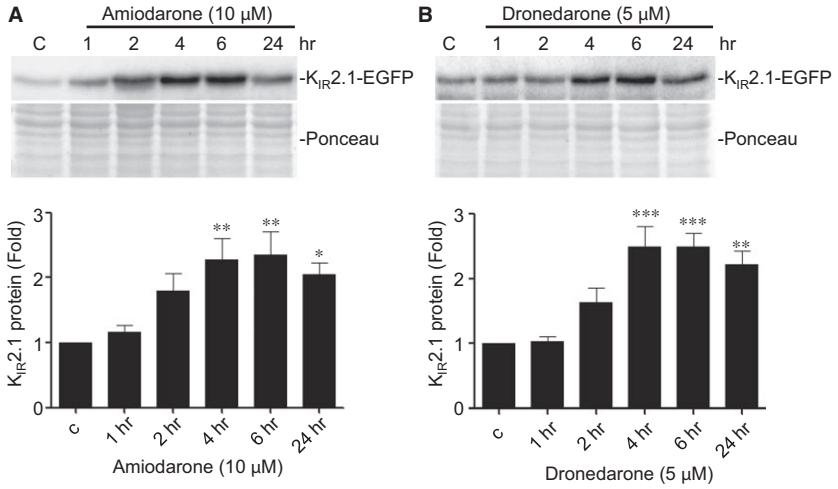


**Fig. 4** Amiodarone and dronedarone induce time-dependent increases in $K_{IR}2.1$-GFP expression. Western blot analysis of $K_{IR}2.1$-GFP expression in HK-KWGF cells treated for 1, 2, 4, 6 and 24 hrs with 10 μM amiodarone or 5 μM dronedarone. C indicates control (untreated) cells. Ponceau staining is used as loading control. Averaged data from eight (amiodarone) and ten (dronedarone) independent experiments, respectively, are shown in bar graphs in the lower part of both panels. $*P < 0.05$; $**P < 0.01$; $***P < 0.001$.

the occurrence of skeletal muscle vacuolarization with or without the presence of inclusion bodies upon chronic amiodarone therapy, interpreted as lysosomal defects by the authors [37, 38]. In myocardial fibres from the left and right ventricle, and right atrium derived from dogs chronically treated with amiodarone, abnormal lysosomal structures with often dense lamellar inclusion bodies were found [39]. Similar 'autophagic vacuoles' were observed in isolated rat ventricular myocytes chronically treated with amiodarone *in vitro* [40, 41]. Morissette *et al.* demonstrated that amiodarone application resulted in vacuolar sequestration and evolved towards persistent macroautophagy in macrophages, smooth muscle cells and HEK293 cells [42]. Dronedarone shows strong similarities to amiodarone with respect to induction of the formation of cellular vacuoles containing lamellar bodies (lysosomal structures) as demonstrated in alveolar macrophages [43].

We found that amiodarone and dronedarone treatment increased $K_{IR}2.1$ expression and intracellular accumulation, most likely in late endosomes and lysosomes, in several different cell lines. Interestingly, compared with chloroquine treatment that results in lysosomal accumulation of full-length and a discrete N-terminally cleaved $K_{IR}2.1$ protein, only accumulation of the full-length product is seen with amiodarone and dronedarone. Therefore, either the majority of the $K_{IR}2.1$ accumulates in pre-lysosomal compartments, which is in line with the findings of Picolli *et al.* [17] who describe that amiodarone and dronedarone do not affect early endosome function, but interferes in the late compartments of the endocytotic pathway, or these compounds interfere in protease function responsible for the N-terminal $K_{IR}2.1$ cleavage. The latter explanation is in line with findings of Buratta *et al.* [44] who describe that specific cathepsins display altered processing in some cell types upon amiodarone treatment.



Journal of Cellular and Molecular Medicine published by John Wiley & Sons Ltd and Foundation for Cellular and Molecular Medicine.

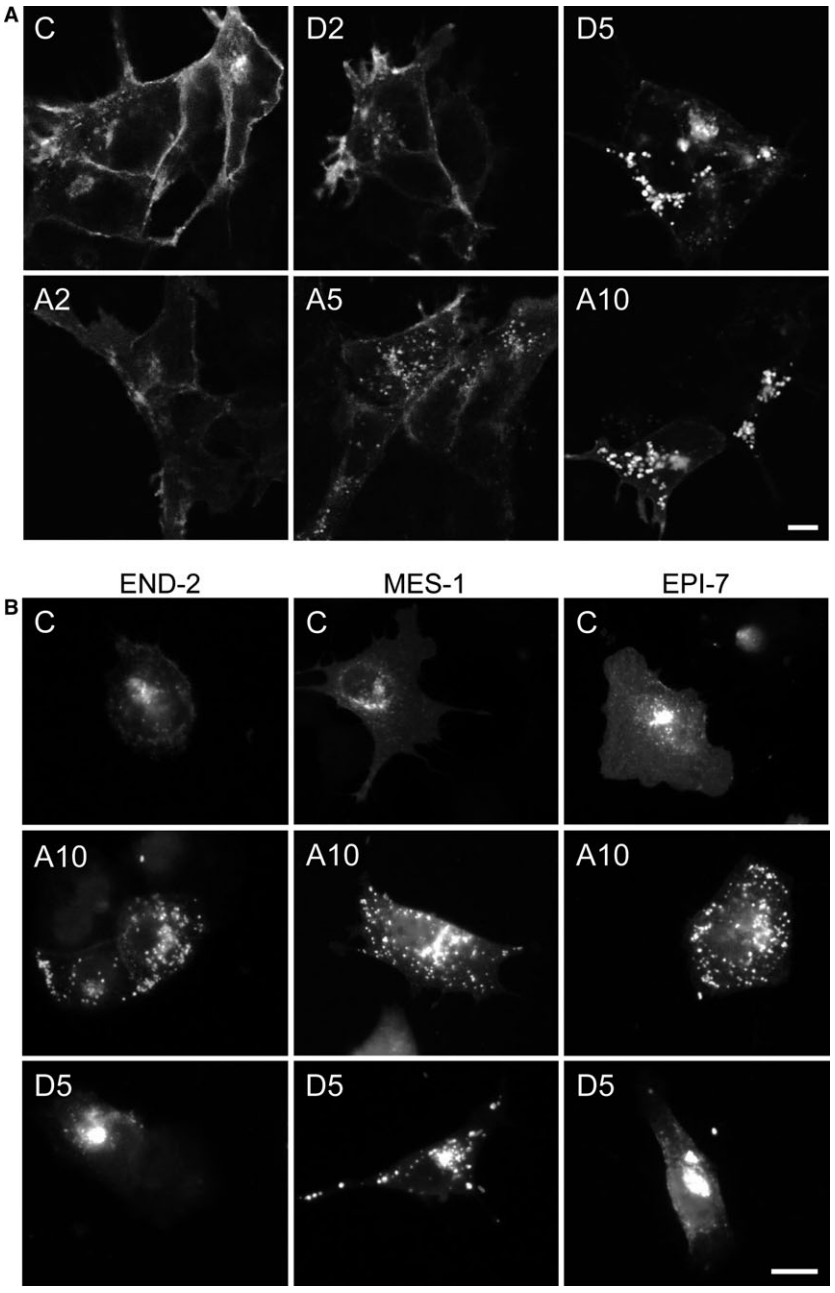


**Fig. 5** Amiodarone and dronedarone induce dose-dependent intracellular $K_{IR}2.1$ accumulation. (**A**) $K_{IR}2.1$-GFP localization in control (C) (untreated) and HK-KWGF cells treated for 24 hrs with 2 (D2) or 5 (D5) μM dronedarone, or 2 (A2), 5 (A5) or 10 (A10) μM amiodarone. (**B**) $K_{IR}2.1$ localization in control (C) (untreated) and END-2, MES-1 and EPI-7 cells treated for 24 hrs with 10 (A10) μM amiodarone or 5 μM (D5) dronedarone**.** Scale bars represent 5 μm.

Whatever the exact mechanism, our findings for $K_{IR}2.1$ are in line with those of Baritussio *et al.* [16], who demonstrated that amiodarone inhibits surfactant protein A degradation that normally takes place in the lysosomal compartment.

As amiodarone treatment correlates with the induction of autophagocytosis, especially upon longer treatment (>24 hrs), we cannot exclude the possibility that a part of the intracellular $K_{IR}2.1$ accumulation occurs in non-functioning, due to the amiodarone and dronedarone acid buffering capacity, macroautophagosomes [42]. This may contribute to the observed colocalization of $K_{IR}2.1$ with LAMP-1. Finally, expression level of the $K_v11.1$ potassium channel protein is not increased by amiodarone or dronedarone, once more demonstrating channel specificity in trafficking pathways and their (patho)physiological regulation [45].

When considering potassium ion channel trafficking with respect to the action of amiodarone and dronedarone, only few data are

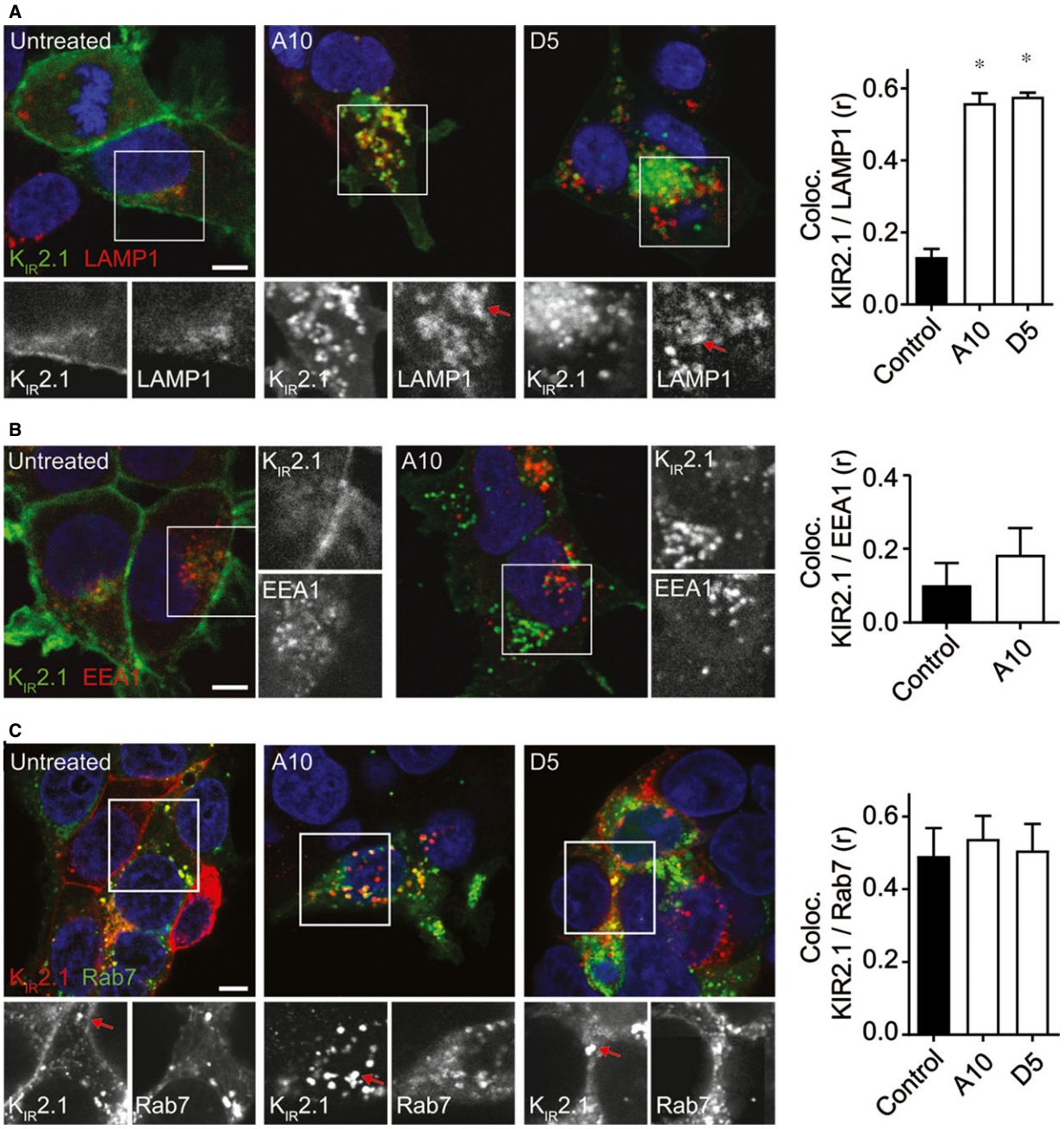


**Fig. 6** (**A**) Costaining of $K_{IR}2.1$-GFP and LAMP1 in control (untreated) and cells treated with 10 μM amiodarone (A10) or 5 μM dronedarone (D5). Merged pictures are presented in colour. Individual staining patterns of the boxed parts are given in the lower six panels in b/w. Red arrows indicate regions of colocalization. Pearson coefficient of colocalization is presented as bars on the right. (**B**) Costaining of $K_{IR}2.1$-GFP (green) and EEA1 (red) in control (untreated) and cells treated with 10 μM amiodarone (A10). Individual staining patterns of the boxed parts are given in the right panels in b/w. Pearson coefficient of colocalization is presented as bars on the right. (**C**) Costaining of $K_{IR}2.1$ (red) and Rab7-GFP (green) in control (untreated) and cells treated with 10 μM amiodarone (A10) or 5 μM dronedarone (D5). Individual staining patterns of the boxed parts are given in the lower six panels in b/w. Pearson coefficient of colocalization is presented as bars on the right. Scale bars represent 5 μm. $*P < 0.05$.



Journal of Cellular and Molecular Medicine published by John Wiley & Sons Ltd and Foundation for Cellular and Molecular Medicine.

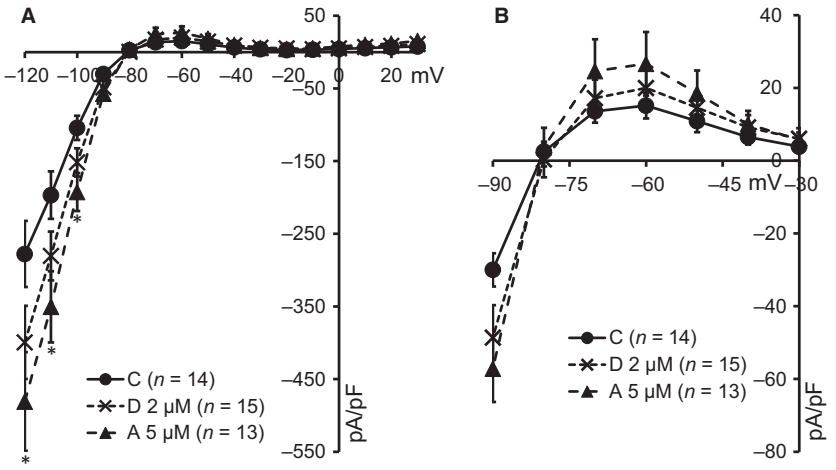


**Fig. 7** Twenty four-hours treatment with amiodarone and dronedarone increases functional $K_{IR}2.I$ expression. (**A**) Current–voltage relationship of $I_{KIR2.1}$ in control cells (C) (filled circles, $N = 14$) and cells treated with either 2 μM dronedarone (D) (crosses, $N = 15$) or 5 μM amiodarone (A) (triangles, $N = 13$). *Amiodarone effects reach significance ($P < 0.05$) at −120, −110 and −100 mV. (**B**) Enlargement of panel A from membrane voltage between −90 and −30 mV indicating a trend in outward current increase upon amiodarone and dronedarone treatment.

available in the literature. Taniguchi *et al.* [46] found no effect of amiodarone on $I_{Ks}$ channel trafficking in Chinese hamster ovary cells. In the hERG-Lite assay [47], amiodarone inhibits hERG surface expression which may result from impaired forward or enhanced backward trafficking or translation interference. We and others showed that backward trafficking of hERG and $K_{IR}2.1$ channels follows different pathways, which makes them react differently to a number of drugs [11]. We showed that amiodarone and dronedarone also affect $K_{IR}2.1$ trafficking differently than that for hERG channels. In cardiomyocytes isolated from guinea pigs treated with amiodarone for 7 days, decreased $I_{K1}$, $I_{Ks}$ and $I_{Kr}$ densities were found [48]. In contrast, in cardiomyocytes from mice treated with amiodarone for 6 weeks, no differences in $I_{K1}$ densities, in neither *KCNJ2* nor *KCNJ12* transcript levels, were observed [49]. For now, it is unclear to what extent and by what mechanisms amiodarone and dronedarone affect potassium ion channel trafficking *in vivo* which warrants future research.

## Acknowledgements

We thank Laura G. Freriks and Ralph G. Tieland for their helpful contributions at the early stages of the current studies. We thank Craig T. January (University of Wisconsin, USA) for providing HEK-hERG cells, Nenad Bursac (Duke University, Durham, USA) for providing Ex293 cells and Christine Mummery (Hubrecht Laboratory, Utrecht, Netherlands) for providing END-2, MES-1 and EPI-7 cells. The research leading to the results has received funding from EU project 'increasing of the R&D capacity at Charles University through new positions for graduates of doctoral studies' CX.1.07/2.3.00/30.0061: Utrecht University Focus and Massa Program Nanobullets; Y.J. and M.Q. are recipients of a scholarship from the Chinese Scholarship Council.

## Conflict of interest

The authors confirm that there are no conflict of interests.

## References

1. **Hibino H, Inanobe A, Furutani K, *et al.*** Inwardly rectifying potassium channels: their structure, function, and physiological roles. *Physiol Rev*. 2010; 90: 291–366.
2. **Nguyen HL, Pieper GH, Wilders R.** Andersen-Tawil syndrome: clinical and molecular aspects. *Int J Cardiol*. 2013; 170: 1–16.
3. **Veldhuis MG, Ji Y, Van der Heyden MAG.** A little too much: cardiac electrophysiological effects of elevated inward rectifying current carried by the $K_{IR}2.1$ ion channel protein. *Adapt Med*. 2015; 7: 1–8.
4. **De Boer TP, Houtman MJ, Compier M, *et al.*** The mammalian $K_{IR}2.x$ inward rectifier ion channel family: expression pattern and pathophysiology. *Acta Physiol (Oxf)*. 2010; 199: 243–56.
5. **Zhang L, Benson DW, Tristani-Firouzi M, *et al.*** Electrocardiographic features in Andersen-Tawil syndrome patients with KCNJ2 mutations: characteristic T-U-wave patterns predict the KCNJ2 genotype. *Circulation*. 2005; 111: 2720–6.
6. **Bhoelan BS, Stevering CH, van der Boog AT, *et al.*** Barium toxicity and the role of the potassium inward rectifier current. *Clin Toxicol (Phila)*. 2014; 52: 584–93.
7. **Postema PG, Ritsema van Eck HJ, Opthof T, *et al.*** $I_{K1}$ modulates the U-wave: insights in a 100-year-old enigma. *Heart Rhythm*. 2009; 6: 393–400.
8. **De Git KC, De Boer TP, Vos MA, *et al.*** Cardiac ion channel trafficking defects and drugs. *Pharmacol Ther*. 2013; 139: 24–31.
9. **Jansen JA, De Boer TP, Wolswinkel R, *et al.*** Lysosome mediated Kir2.1 breakdown directly influences inward rectifier current density. *Biochem Biophys Res Commun*. 2008; 367: 687–92.
10. **Varkevisser R, Houtman MJ, Waasdorp M, *et al.*** Inhibiting the clathrin-mediated endocytosis pathway rescues $K_{IR}2.1$ downregulation by pentamidine. *Pflugers Arch*. 2013; 465: 247–59.
11. **Nalos L, De Boer TP, Houtman MJ, *et al.*** Inhibition of lysosomal degradation rescues pentamidine-mediated decreases of $K_{IR}2.1$ ion channel expression but not that of $K_v11.1$. *Eur J Pharmacol*. 2011; 652: 96–103.
12. **Punnam SR, Goyal SK, Kotaru VP, *et al.*** Amiodarone - a 'broad spectrum'

antiarrhythmic drug. *Cardiovasc Hematol Disord Drug Targets*. 2010; 10: 73–81.

13. **Vorperian VR, Havighurst TC, Miller S, *et al.*** Adverse effects of low dose amiodarone: a meta-analysis. *J Am Coll Cardiol*. 1997; 30: 791–8.
14. **Vassallo P, Trohman RG.** Prescribing amiodarone. An evidence-based review of clinical indications. *JAMA*. 2007; 298: 1312–22.
15. **Santangeli P, Di Biase L, Burkhardt JD, *et al.*** Examining the safety of amiodarone. *Expert Opin Drug Saf*. 2012; 11: 191–214.
16. **Baritussio A, Marzini S, Agostini M, *et al.*** Amiodarone inhibits lung degradation of SP-A and perturbs the distribution of lysosomal enzymes. *Am J Physiol Lung Cell Mol Physiol*. 2001; 281: 1189–99.
17. **Piccoli E, Nadai M, Caretta CM, *et al.*** Amiodarone impairs trafficking through late endosomes inducing a Niemann-Pick C-like phenotype. *Biochem Pharmacol*. 2011; 82: 1234–49.
18. **Shaikh NA, Downar E, Butany J.** Amiodarone – an inhibitor of phospholipase activity: a comparative study of the inhibitory effects of amiodarone, chloroquine and chlorpromazine. *Mol Cell Biochem*. 1987; 76: 163–72.
19. **Patel C, Yan GX, Kowey PR.** Dronedarone. *Circulation*. 2009; 120: 636–44.
20. **Friart J, Rasson G.** Etude des modifications de l'électrocardiogramme provoquées par l'amiodarone. *Arzneimittelforschung*. 1971; 21: 1535–41.
21. **Rosenbaum MB, Chiale PA, Ryba D, *et al.*** Control of tachyarrhythmias associated with Wolff-Parkinson-White syndrome by amiodarone hydrochloride. *Am J Cardiol*. 1974; 34: 215–23.
22. **Rosenbaum MB, Chiale PA, Halpern MS, *et al.*** Clinical efficacy of amiodarone as an antiarrhythmic agent. *Am J Cardiol*. 1976; 38: 934–44.
23. **Nalos L, Varkevisser R, Jonsson MK, *et al.*** Comparison of the $I_{Kr}$ blockers moxifloxacin, dofetilide and E-4031 in five screening models of pro-arrhythmia reveals lack of specificity of isolated cardiomyocytes. *Br J Pharmacol*. 2012; 165: 467–78.
24. **De Boer TP, Van Veen TA, Houtman MJ, *et al.*** Inhibition of cardiomyocyte automaticity by electrotonic application of inward rectifier current from Kir2.1 expressing cells. *Med Biol Eng Comput*. 2006; 44: 537–42.
25. **Mummery CL, Feijen A, Van der Saag PT, *et al.*** Clonal variants of differentiated P19 embryonal carcinoma cells exhibit epidermal growth factor receptor kinase activity. *Dev Biol*. 1985; 109: 402–10.
26. **Mummery CL, Feijen A, Moolenaar WH, *et al.*** Establishment of a differentiated mesodermal line from P19 EC cells expressing functional PDGF and EGF receptors. *Exp Cell Res*. 1986; 165: 229–42.
27. **Zhou Z, Gong Q, Epstein ML, *et al.*** HERG channel dysfunction in human long QT syndrome. Intracellular transport and functional defects. *J Biol Chem*. 1998; 273: 21061–6.
28. **Kirkton RD, Bursac N.** Engineering biosynthetic excitable tissues from unexcitable cells for electrophysiological and cell therapy studies. *Nat Commun*. 2011; 2: 300.
29. **Bolte S, Cordelières FP.** A guided tour into subcellular colocalization analysis in light microscopy. *J Microsc*. 2006; 224: 213–32.
30. **Sato R, Koumi S, Singer DH, *et al.*** Amiodarone blocks the inward rectifier potassium channel in isolated guinea pig ventricular cells. *J Pharmacol Exp Ther*. 1994; 269: 1213–9.
31. **Gautier P, Guillemare E, Marion A, *et al.*** Electrophysiologic characterization of dronedarone in guinea pig ventricular cells. *J Cardiovasc Pharmacol*. 2003; 41: 191–202.
32. **Holt DW, Tucker GT, Jackson PR, *et al.*** Amiodarone pharmacokinetics. *Am Heart J*. 1983; 106: 840–7.
33. **Milstein ML, Musa H, Balbuena DP, *et al.*** Dynamic reciprocity of sodium and potassium channel expression in a macromolecular complex controls cardiac excitability and arrhythmia. *Proc Natl Acad Sci USA*. 2012; 109: E2134–43.
34. **Van der Heyden MA, Defize LH.** Twenty one years of P19 cells: what an embryonal carcinoma cell line taught us about cardiomyocyte differentiation. *Cardiovasc Res*. 2003; 58: 292–302.
35. **Lewis JH, Mullick F, Ishak KG, *et al.*** Histopathologic analysis of suspected amiodarone hepatotoxicity. *Hum Pathol*. 1990; 21: 59–67.
36. **Papiris SA, Triantafillidou C, Kolilekas L, *et al.*** Amiodarone. Review on pulmonary effects and toxicity. *Drug Saf*. 2010; 33: 539–58.
37. **Meier C, Kauer B, Müller U, *et al.*** Neuromyopathy during chronic amiodarone treatment. *J Neurol*. 1979; 220: 231–9.
38. **Fernando Roth R, Itabashi H, Louie J, *et al.*** Amiodarone toxicity: myopathy and neuropathy. *Am Heart J*. 1990; 119: 1223–5.
39. **Gross SA, Somani P.** Amiodarone-induced ultrastructural changes in canine myocardial fibers. *Am Heart J*. 1986; 112: 771–9.
40. **Yang YZ, Yang XY, Guo Q, *et al.*** Cytotoxic effects of changrolin, lidocaine and amiodarone on ultrastructure of cultured rat beating cardiac myocytes. *Acta Pharmacol Sin*. 1989; 10: 46–8.
41. **Nag AC, Lee ML, Shepard D.** Effect of amiodarone on the expression of myosin isoforms and cellular growth of cardiac muscle cells in culture. *Circ Res*. 1990; 67: 51–60.
42. **Morissette G, Ammoury A, Rusu D, *et al.*** Intracellular sequestration of amiodarone: role of vacuolar ATPase and macroautophagic transition of the resulting vacuolar cytopathology. *Br J Pharmacol*. 2009; 157: 1531–40.
43. **Quaglino D, Ha HR, Duner E, *et al.*** Effects of metabolites and analogs of amiodarone on alveolar macrophages: structure-activity relationship. *Am J Physiol Lung Cell Mol Physiol*. 2004; 287: L438–47.
44. **Buratta S, Urbanelli L, Ferrara G, *et al.*** A role of the autophagy regulator Transcription Factor EB in amiodarone-induced phospholipidosis. *Biochem Pharmacol*. 2015; 95: 201–9.
45. **Varkevisser R, Houtman MJ, Linder T, *et al.*** Structure-activity relationships of pentamidine-affected ion channel trafficking and dofetilide mediated rescue. *Br J Pharmacol*. 2013; 169: 1322–34.
46. **Taniguchi T, Uesugi M, Arai T, *et al.*** Chronic probucol treatment decreases the slow component of the delayed-rectifier potassium current in CHO cells transfected with KCNQ1 and KCNE1: a novel mechanism of QT prolongation. *J Cardiovasc Pharmacol*. 2012; 59: 377–86.
47. **Wible BA, Hawryluk P, Ficker E, *et al.*** HERG-Lite: a novel comprehensive high-throughput screen for drug-induced hERG risk. *J Pharmacol Toxicol Methods*. 2005; 52: 136–45.
48. **Bosch RF, Li GR, Gaspo R, *et al.*** Electrophysiologic effects of chronic amiodarone therapy and hypothyroidism, alone and in combination, on guinea pig ventricular myocytes. *J Pharmacol Exp Ther*. 1999; 289: 156–65.
49. **Le Bouter S, El Harchi A, Marionneau C, *et al.*** Long-term amiodarone administration remodels expression of ion channel transcripts in the mouse heart. *Circulation*. 2004; 110: 3028–35.



Journal of Cellular and Molecular Medicine published by John Wiley & Sons Ltd and Foundation for Cellular and Molecular Medicine.